Journal of Power Sources 196 (2011) 9648–9653

Contents lists available at ScienceDirect

Journal of Power Sources

journal homepage: www.elsevier.com/locate/jpowsour

Composite electrodes of disordered carbon and graphite for improved battery state estimation with minimal performance penalty

John S. Wang[a,*], Elena Sherman[a], Mark Verbrugge[b], Ping Liu[a]

[a] Sensors and Materials Lab, HRL Laboratories LLC, Malibu, CA, United States
[b] Chemical Sciences and Materials Systems Lab, General Motors Research and Development, Warren, MI, United States

ARTICLE INFO

Article history:
Received 1 June 2011
Received in revised form 6 July 2011
Accepted 7 July 2011
Available online 29 July 2011

Keywords:
Lithium ion battery
State of charge
SOC
Mixed composite electrode
Battery state estimation

ABSTRACT

Voltage based state of charge (SOC) estimation is challenging for lithium ion batteries that exhibit little open circuit voltage (OCV) change over a large SOC range. We demonstrate that by using a composite negative electrode composed of disordered carbon and graphite, we were able to introduce additional features to the OCV–SOC relationship that facilitate voltage-based SOC estimation. In contrast to graphite, the potential of disordered carbon is sensitive to the state of charge; this behavior, when manifested in a lithium ion battery, gives rise to additional beneficial features of the cell OCV–SOC relationship in terms of state estimation. We have demonstrated the effectiveness of the approach by comparing model simulations and corresponding experimental data of a cell composed of $LiFePO_4$ positives and graphite + disordered carbon composite negative electrodes. Last, we find that although the graphite material has a higher coulombic capacity, very little (dynamic) performance loss is manifest with the mixed graphite + disordered carbon composite is employed.

1. Introduction

Efficient energy management is important for realizing the full benefit of lithium ion batteries in hybrid and electric vehicles. An important component of the system is an adaptive algorithm that provides real time prediction of state of charge (SOC), state of health (SOH), and available power [1]. For SOC prediction, a combination of a charge-based SOC with a voltage-based SOC is often employed. The voltage-based SOC is obtained by first estimating the open-circuit voltage (OCV) and applying it to a predetermined OCV–SOC relation. Unlike the charge-based SOC, the voltage-based SOC algorithm can be calibrated to respond quickly to minimize the error between the model voltage and the measured voltage. The voltage-based SOC is an integral part of an adaptive SOC algorithm because of its ability to minimize the errors in real time adaptive fashion.

Voltage-based SOC estimation is extremely challenging when the cell potential remains substantially unchanged over a broad SOC range (e.g., from 10 to 90% SOC). For these batteries, small errors in OCV estimation can result in very large errors in SOC estimation [2]. This examines a state estimator for NiMH, which has a flat SOC–OCV relation, and highlights the problems mentioned here. An example is a lithium ion battery with a $LiFePO_4$ positive and a graphite negative electrode. This battery is a promising candidate for high power applications such as for use in hybrid electric vehicles (HEVs) and power tools because of high thermal stability, relatively low cost, and reported long cycle life [3–12]. The system is also of interest for plug-in HEV and extended-range electric vehicle applications. Consequently, it is highly desirable to develop a solution to improve the estimation of voltage based SOC for this battery in order to facilitate its implementation in automotive applications.

In previous work, we employed $LiFePO_4$ as the positive and a mixture of lithium titanate (LTO) and a graphitic carbon as the negative electrode [13]. During battery discharge, lithium is first removed from graphite between 0 and 0.2 V (vs. a Li reference) and then from LTO at about 1.5 V. This difference in the OCVs of the graphite and LTO produces an abrupt change in cell voltage and provides an early warning, in terms of state estimation, before the battery reaches the end of discharge. This composite design requires LTO to cycle reversibly down to near the potential of lithium metal. In addition, during lithium insertion and extraction from LTO, the actual rate can be very high since all current will be directed to LTO while graphite is largely inactive in the voltage range near 1.5 V.

In this paper, we extend the concept of using composite materials to modify the shape of the OCV–SOC curve to a negative electrode made of disordered carbon and graphitic carbon. Unlike LTO and graphite, the operating potentials of disordered carbon

* Corresponding author. Tel.: +1 310 317 5155; fax: +1 310 317 5840.
E-mail address: jswang@hrl.com (J.S. Wang).

0378-7753/$ – see front matter © 2011 Elsevier B.V. All rights reserved.
doi:10.1016/j.jpowsour.2011.07.023

and graphite carbon overlap substantially but disordered carbon has a larger variation in potential. Disordered carbon does have a lower specific capacity than graphite but can exhibit excellent cycling stability. Specifically, the OCV of MCMB disordered carbon is sensitive to its SOC [14–16]. Consequently its potential is a good indicator for its SOC. In contrast, graphite delivers most of its usable capacity between 0.2 and 0 V and its OCV is very insensitive to its SOC. A composite anode made of these two carbons will allow us to manipulate the shape of the OCV–SOC profile without a large compromise in storage capacity. In a battery, the cell voltage is the potential difference between the positive and the negative electrodes. Consequently, the OCV–SOC relationship of the negative electrode will influence the OCV–SOC relationship for the battery, especially when the potential of the positive electrode is substantially insensitive to its SOC, such as in the case for $LiFePO_4$.

We will first describe the electrochemical performance of three negative electrodes: graphite, MCMB disordered carbon, and a MCMB/graphite mixed composite. Next, we describe a simple, thermodynamic model for a cell composed of a $LiFePO_4$ positive and carbon negative to illustrate the effect of disordered carbon on the OCV–SOC profile. Last, we show experimental data that validates the model. In characterizing the electrochemical properties, we employ cyclic voltammetry and galvanostatic charge-discharge methods. Overall, our results further confirm that using a mixture of a disordered carbon and graphite provides an effective approach to improve SOC monitoring of lithium ion batteries for improved energy and power management.

2. Experimental

2.1. Electrode preparation

Three different negative electrodes were cast using a doctor-blade technique: graphite (SG, Superior Graphite, SLC 1520), MCMB disordered carbon (MCMB 10-10), and a graphite/MCMB disordered carbon mixed composite (SG/MCMB). The compositions of SG and MCMB electrodes were 93 wt% active carbon material, 3 wt% carbon black (Super P), and 4 wt% SBR binder (an aqueous styrene–butadiene rubber binder, LHB-108P). For the SG/MCMB composite negative electrode, the composition was 74.4 wt% SG, 18.6 wt% MCMB, 3 wt% carbon black and 4 wt% SBR binder. The mass ratio between SG and MCMB is thus 4:1. For the full-cell experimental studies, $LiFePO_4$ was used as the positive electrode which was prepared using the commercially available 2.2 Ah, 26650 cylindrical cells (A123Systems, MA). After disassembling the 26650 cell in an Argon filled glove box, circular disks were punched out of the positive cathode electrode tape and rinsed with dimethyl carbonate (DMC).

2.2. Characterization methods

All the electrochemical experiments were carried out in Swagelok cells inside an Argon filled glovebox. For the half-cell testing, lithium metal was used as the counter electrode. The electrolyte solution was 1 M $LiPF_6$ in 1:1 (v/v) ethylene carbonate (EC) and dimethyl carbonate (DMC). A Celgard 3501 (25 μm thick microporous polypropylene film with 40% porosity) was used as the separator. Galvanostatic studies were performed with an Arbin BT-2000 battery testing station. The cycling voltage ranged from 10 mV to 2 V for the carbon and 2.5–4 V for the $LiFePO_4$ electrode (relative to a Li/Li^+ electrode). The cyclic voltammetry (CV) experiments were carried out using a PAR EG&G 283 potentiostat. The cutoff voltages for the carbon–$FePO_4$ cell were 2.0 and 3.6 V.

3. Results and discussion

3.1. Electrochemical performance of composite carbon negative electrode

Fig. 1 shows the SEM images for three different negative electrodes: MCMB disordered carbon, SG, and SG/MCMB mixed carbon. The carbon particles of MCMB electrode are more densely packed than those of the SG electrode, and the composite electrode appears to be smoother and less porous than the SG electrode. The MCMB disordered carbon particles appear to be complementary to the larger, spherical shaped SG particles in forming a densely packed electrode; the architecture of the composite electrode may promote better electrical contact between particles.

Fig. 2 shows the C/20 galvanostatic charge/discharge voltage responses of the SG, MCMB, and SG/MCMB composite electrodes. As expected, the potential of MCMB gradually decreases with SOC without any plateaus on the charge/discharge profile. In contrast, the SG delivers most of its capacity between 0 and 0.2 V and the electrode potential is less sensitive to SOC. The potential-SOC characteristics of the MCMB electrode material are favorable for SOC estimations since electrode potential is a reliable indicator of SOC. The mixed SG/MCMB electrode inherits the features from both SG and MCMB materials. The electrode potential changes continuously with SOC until reaching about 0.2 V with about 17% of electrode capacity delivered.

The rate capability of MCMB disordered carbon is better than that of SG, as shown in Fig. 3, where cyclic voltammetric (CV) responses of both electrodes are recorded at sweep rates of 1, 0.1, and 0.02 mV s^{-1}. The MCMB electrode reveals a featureless voltammetric response over a broad potential range. The response arises from the numerous lithium intercalation sites with a wide variation in energies, characteristic of single-phase electrodes. These results are consistent with the potential profiles during galvanostatic cycling shown in Fig. 2. In contrast, the SG electrode shows well-defined redox (reduction-oxidation) peaks at slow sweep rates, e.g. 0.02 mV s^{-1}. The peaks represent the co-existence of lithiated graphite compounds of different stages [17]. Each peak corresponds to a plateau region on the (low rate) galvanostatic potential profile. However, the peaks were not visible at 1 mV s^{-1}, indicating poor reaction kinetics due to slow diffusion of lithium ions. Such kinetics effects can also be seen by comparing the charge storage performance at different sweep rates. In CV responses, the area underneath the curves has units of power per unit mass as plotted and reflects the total stored charge. As the sweep rate decreases, the total amount of stored charge increases. At a sweep rate of 1 mV s^{-1}, the total stored lithium capacity (anodic process) for MCMB disordered carbon was calculated to be 135 mAh s^{-1} (55% of its full capacity) while the SG electrode only stored 27 mA h g^{-1} (7% of its full capacity). These results are consistent with the MCMB disordered carbon material exhibiting faster lithium intercalation/deintercalation kinetics than the SG material.

Fig. 4 shows a comparison of charge capacity at C/4, C/2, and 2C rates for MCMB disordered carbon, SG, and the SG/MCMB composite electrode. At the 2C rate, the charge capacity of MCMB fades very slightly with cycling while that of SG fades significantly. The superior high charge rate capabilities of MCMB disordered carbon are likely related to its structural architecture. Disordered carbon materials such as MCMB have a large d_{002} spacing, typically about 0.37 nm [15]. Consequently, MCMB can accommodate lithium between the layers with minimal structural deformation. Graphite, in comparison, has a smaller d_{002} spacing (0.34 nm). The spacing increases up to 10% during lithium intercalation. Such structural change can potentially hinder both the rate capability and cycling stability. Therefore, adding MCMB disordered carbon to SG also improves its charge rate capability (Fig. 4).

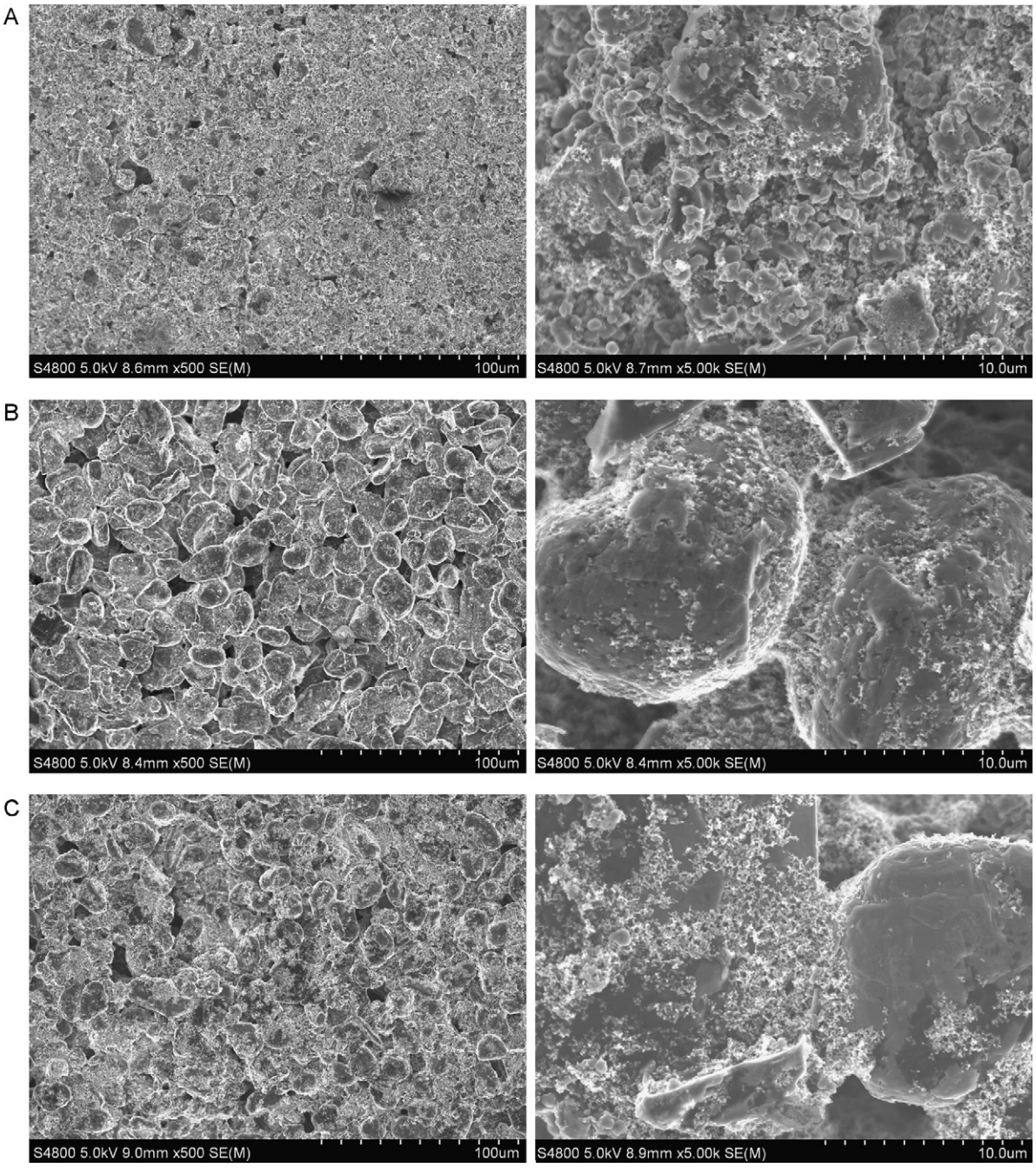

Fig. 1. SEM images of negative electrodes: (A) MCMB disordered carbon only; (B) graphite (SG) only; (C) SG/MCMB (80/20 wt%) mixed composite.

Fig. 5 shows a comparison of cycling performance of SG, MCMB disordered carbon, and the SG/MCMB composite electrodes at C/4 rate. The cycling performance of all three material compositions is excellent. However, the charge capacity of MCMB disordered carbon electrode is only at 205 mA h g^{-1} as compared to a charge capacity of 370 mA h g^{-1} for SG. For the 80:20 wt% ratio SG:MCMB mixed electrode, the charge capacity was above 350 mA h g^{-1}. The charge capacity of the mixed composite electrode is slightly higher than a summation of the expected capacities from the two components at C/4 rate. While this can be considered within experimental error, it is possible that the mixed composite electrode improves the utilization of the disorder carbon due to its dispersion in a graphite matrix thus enhancing its rate capability. These results are consistent with previous findings that the mixture of graphite and coke enhanced discharge capacity and cycling performance as compared to the sum of the capacities for each individual material; enhanced electrical conductivity of the mixture was suggested for the improvement [14].

3.2. Composite carbon negative and state estimation of lithium-ion cells

To illustrate the concept of using the SG/MCMB mixture to improve SOC estimation, we first build a model to simulate the discharge characteristics of a cell when it is paired with a $LiFePO_4$ positive. Fig. 6 shows simulated galvanostatic discharge profiles of two cells: (1) a $LiFePO_4$ positive versus SG/MCMB (80/20 wt%) negative electrode and (2) a $LiFePO_4$ positive versus SG only negative electrode. The cell potential is the experimentally measured equilibrium voltage of the positive electrode minus that of nega-

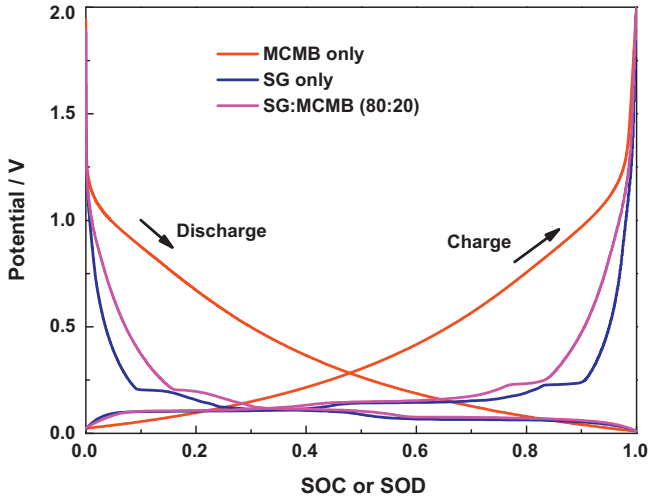

Fig. 2. Galvanostatic discharge and charge curves of MCMB disordered carbon, SG, and SG/MCMB composite electrodes at a C/20 rate. Lithium metal was used as a counter electrode for all the cells.

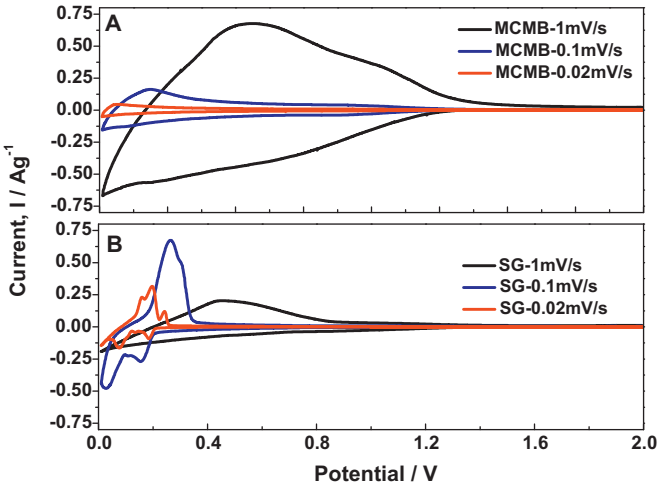

Fig. 3. Cyclic voltammetric responses of MCMB disordered carbon (A) and SG (B) electrodes at the various sweep rates: 1, 0.2, and 0.02 mV s^{-1}.

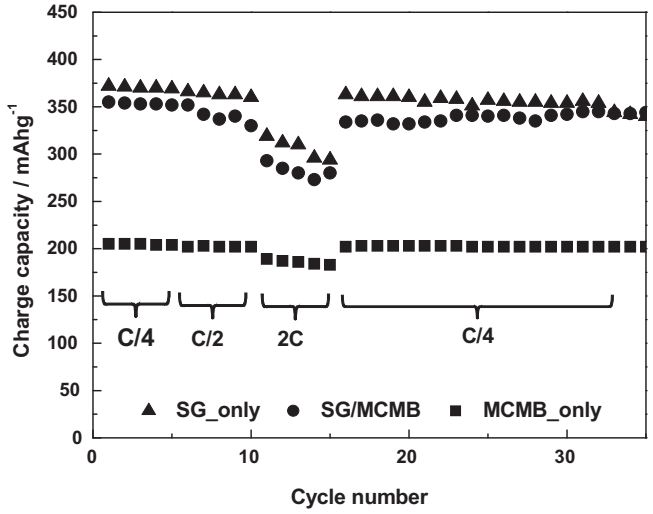

Fig. 4. Charge capacities of MCMB disordered carbon, SG, and SG/MCMB composite electrodes as a function of cycle number at various galvanostatic charge rates: C/4, C/2 and 2C.

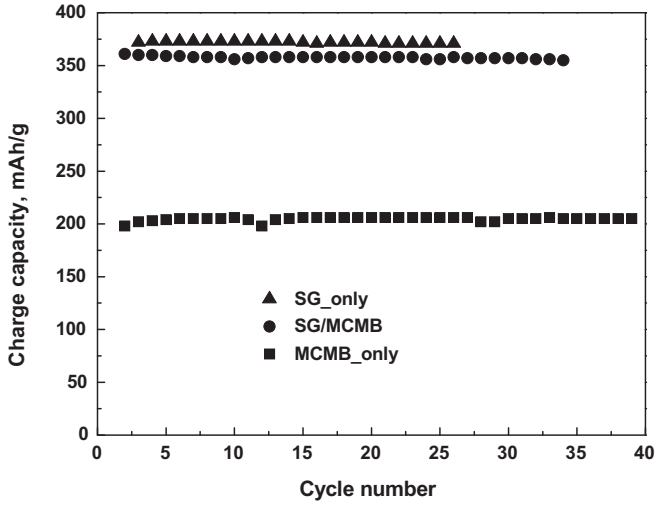

Fig. 5. Specific charge capacities as a function of cycle number for three type of negative electrodes: MCMB disordered carbon, SG, and SG/MCMB composite.

tive electrode. As shown in Fig. 6, the addition of MCMB disordered carbon creates a sloping OCV–SOC curve near the end of discharge as compared to the SG only electrode, for which the voltage drops abruptly at the end of discharge. In addition, the voltage profiles are tunable by adjusting the SG and MCMB weight ratio. The composite negative electrode provides a gradual potential drop that signals impending end of discharge. The results indicate that the increased variation of the cell OCV–SOC towards the end of discharge can enhance the accuracy of voltage-based SOC estimation.

A cell composed of $LiFePO_4$ positive and SG/MCMB mixed composite negative was constructed to validate our model simulation. Galvanostatic charge/discharge profiles obtained at C/20 rate are shown in Fig. 7. The profiles are in excellent agreement with our simulation, demonstrating that mixing MCMB disordered carbon in the negative electrode can create a clear SOC marker before the end of discharge for the battery.

In order to understand whether the two materials in the same electrode have non-ideal interactions with each other, we subsequently examined whether the voltage profile of the composite electrode can be represented by a straight-forward combination of voltage profiles of the individual components (graphite and MCMB

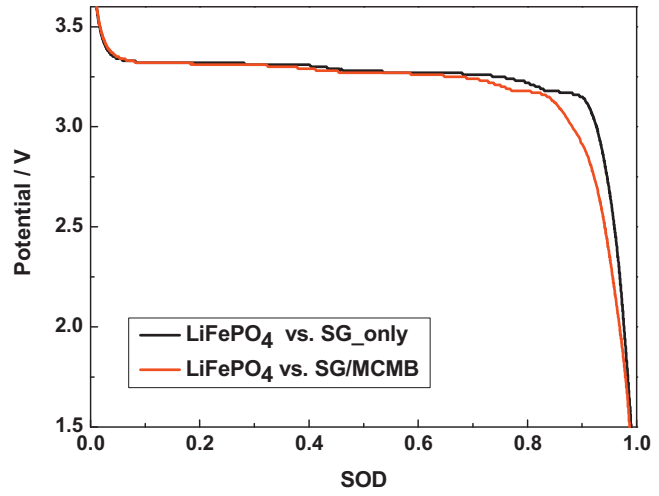

Fig. 6. Simulated discharge profiles of two cells: one composed of $LiFePO_4$ positive and SG/MCMB composite negative electrode; and the second composed of $LiFePO_4$ positive and SG negative electrode.

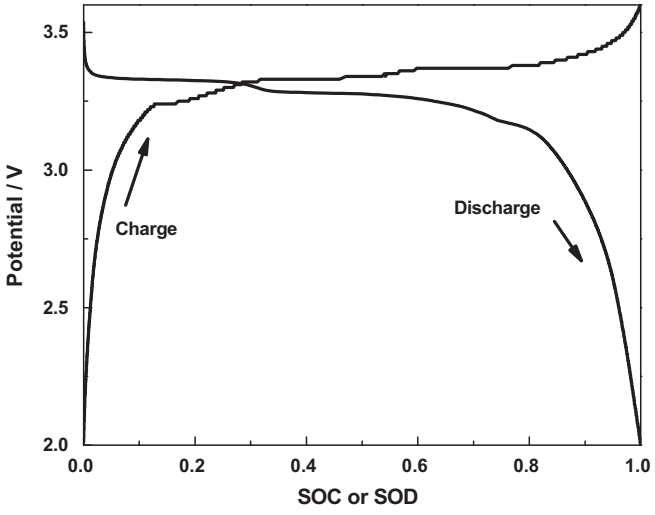

Fig. 7. Galvanostatic charge/discharge curves for a cell with a $LiFePO_4$ positive and the SG/MCMB composite negative at a C/20 rate.

disordered carbon). The charge/discharge curves of the composite SG/MCMB negative electrode was simulated by using the galvanostatic charge/discharge voltage responses of SG vs. Li and MCMB vs. Li at C/20 rate (Fig. 2) and compared to the experimentally measured ones. The resistance is deemed to be negligible at such low rate. The combined SOC can be expressed as

$$\mathrm{SOC} = \frac{Q_{\mathrm{SG}}}{Q}\mathrm{SOC}_{\mathrm{SG}} + \frac{Q_{\mathrm{MCMB}}}{Q}\mathrm{SOC}_{\mathrm{MCMB}}$$

where Q_{SG} and Q_{MCMB} are the capacities of SG and MCMB disordered carbon components, respectively, and SOC_{SG} and SOC_{MCMB} are the state-of-charge values for the SG and the MCMB disordered carbon components, respectively. The total capacity of the combined electrode Q corresponds to $Q_{SG} + Q_{MCMB}$. Fig. 8 shows the comparison of charge/discharge curves calculated using the above equation with the experimental data for SG/MCMB composite electrode. The two profiles are very similar, confirming that there is no observable voltage interference (i.e., unexplained behavior) between the SG and MCMB disordered carbon in a composite electrode.

While the above analysis demonstrates that mixing MCMB disordered carbon can enhance the accuracy of voltage based SOC

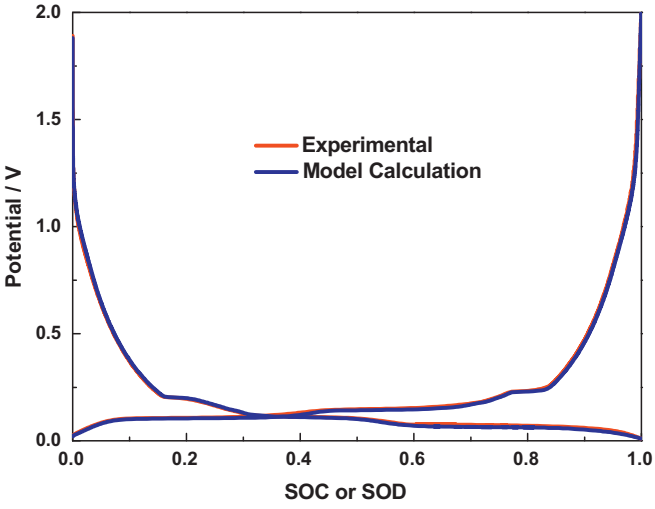

Fig. 8. Comparison of model calculation and experimental charge/discharge curves for SG/MCMB composite electrode at a C/20 rate. Lithium metal was used as counter electrode.

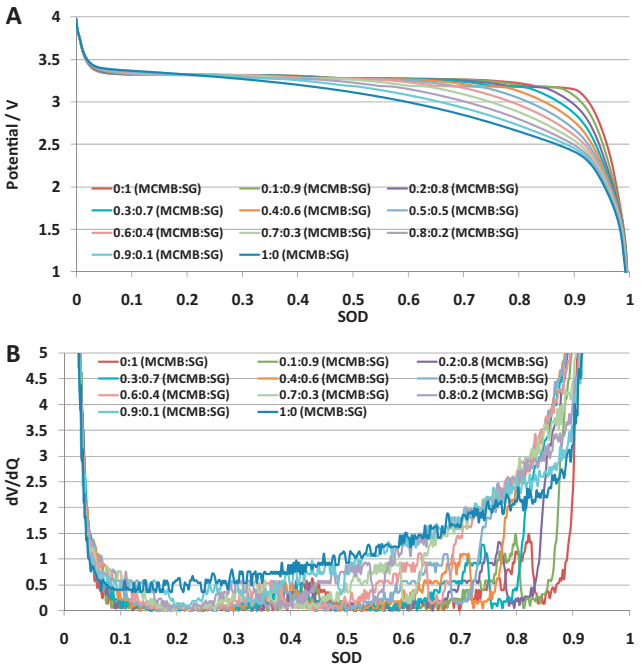

Fig. 9. Simulation results of cells comprised of $LiFePO_4$ positive and SG/MCMB composite negative electrode at various mass fractions of MCMB. (A) discharge profiles; (B) dV/dQ differential curves of the corresponding discharge profiles.

estimations by creating clear SOC markers, it is important to determine how the SOC marker changes with MCMB to SG ratios for application purposes. When the battery is used to power an electric vehicle, the remaining SOC or capacity can be used to estimate the mileage the vehicle can provide before reaching end of discharge. Fig. 9A shows simulation results of cells comprising a $LiFePO_4$ positive and a SG/MCMB composite negative with various SG and MCMB mass ratios. As the mass fraction of MCMB disordered carbon increases, the slopping voltage region towards the end of discharge encompasses a wider range of SOC. Another method to quantitatively identify this mass-ratio dependent SOC–OCV relationship is by constructing dV/dQ differential curves (Fig. 9B). As the mass fraction of MCMB disorder carbon decreases, a dV/dQ peak towards the end of discharge becomes visible. The dV/dQ peak represents the lithium deintercalation (extraction) from graphite during the stage II–III phase transformation. Its peak shift is consistent with the increase of the mass ratio of graphite. Fig. 10 illustrates an example of using both the OCV–SOD relationship and the dV/dQ differential curve as the SOC markers to determine how much capacity or energy remains in a battery. In the slopping voltage region near the end of discharge, such as when OCV = 3.0 V, OCV–SOD relationship can be very effective to identify the SOC. In addition, the dV/dQ peak of the graphite stage II–III phase transformation can also be a clear SOC indicator as shown in Fig. 10.

Finally, we implement voltage marker on the OCV–SOD relation (at OCV = 3.0 V) and a dV/dQ peak from the differential curve to determine the miles of reserve upon reaching these markers for a battery-powered electric vehicle. Our calculations were based on a 40 kW h battery pack and a vehicle energy consumption of 200 W h mile^{-1}. Fig. 11 shows a summary of the results for various mass fraction of MCMB disordered carbon. The specific capacity of the composite negative electrode (mA h g^{-1}) and the specific energy of a packaged cell (W h kg^{-1}) are plotted as function of mass fraction of MCMB disordered carbon (the primary y-axis on the left). The specific energy densities at various mass fraction of MCMB disordered carbon were calculated based on a packaged cell in which the cathode capacity is150 mA h g^{-1} and the cell packing efficiency

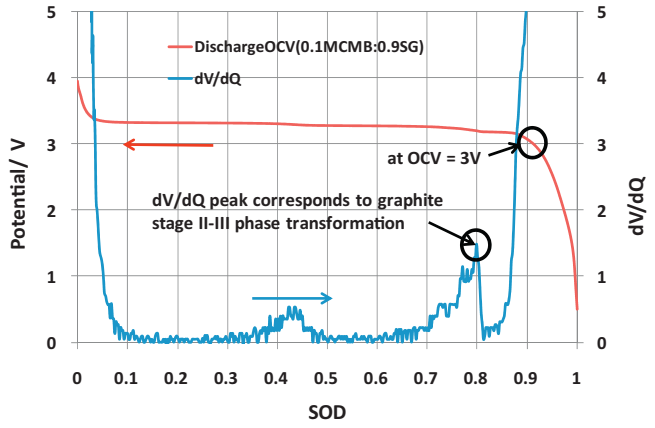

Fig. 10. An illustration of using OCV-SOD relationship and the associated d*V*/d*Q* differential curve to identify the SOC markers (circled). One example uses the OCV at 3.0 V. The other example uses the peak (near 0.8 SOD) on the d*V*/d*Q* curve, which represents the graphite stage II–III phase transformation.

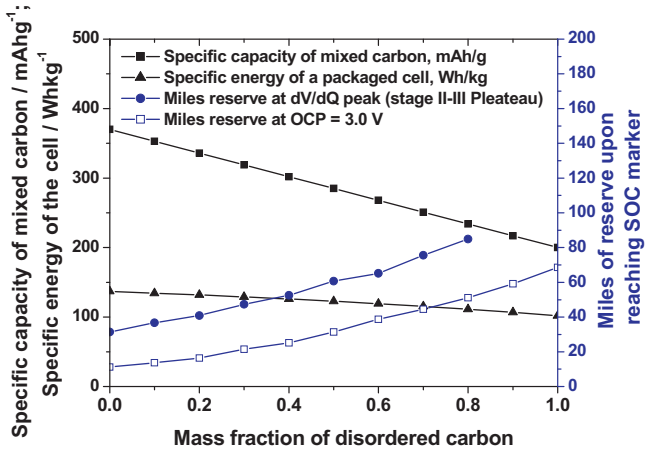

Fig. 11. A summary of specific capacity, energy density and miles of reserve upon reaching SOC markers (described in Fig. 10) plotted as a function of MCMB mass fraction. Miles of reserve directly correlate with how the SOC markers change with the MCMB to SG ratios. The calculations were based on a 40 kW h battery pack with an energy consumption rate of 200 Wh mile^{-}.

is 40% (estimated based on a state of the art prismatic cell). To streamline the analysis and exposition, the cathode to anode capacity ratio was kept at 1:1 (a 5–10% excess in the anode capacity is common in practice). Because MCMB has a lower capacity than that of SG graphite, the specific capacity decreases as the mass fraction of MCMB increases. Thus, the amount of MCMB disordered carbon should be minimized in order to achieve higher energy densities. On the other hand, because the total mass of active carbon at the negative electrode contributes a small fraction of the weight of a packaged cell, the mass fraction of MCMB disordered carbon does not substantially impact the specific energy of the cell (Fig. 11). The miles of reserve upon reaching the SOC markers are plotted on the secondary *y*-axis on the right. Consistent with the above discussion, the miles of reserve increase with increasing MCMB to SG ratios. These results further demonstrate that one can design a battery with a preselected mile reserve by tuning the ratio of disordered carbon to graphite.

4. Summary and conclusions

We have constructed and analyzed an SG (graphite from Superior Graphite)/MCMB (mesocarbon microbead disordered carbon) mixed composite negative electrode. The composite electrode has been shown to exhibit good rate capability and cycling stability. The thermodynamic charge/discharge behavior, corresponding to the OCV versus SOC relation, of the SG/MCMB mixed electrode reveals a significant sloping voltage region near the end of discharge. When the composite negative electrode is implemented in lithium ion batteries with $LiFePO_4$ as the positive electrode, the sloping voltage towards the end of discharge improves the sensitivity of OCV–SOC relation and thereby enhances voltage-based SOC estimation; this observation is particularly relevant for lower states of charge, wherein control of the battery is most important in terms of alerting the user of the impending loss of discharge power capability. Through the comparison of experimental data with thermodynamic simulations, we show that a straightforward application of the component OCV relations can be used to formulate the composite SG/MCMB equilibrium potential. A wide range of MCMB to SG ratios is feasible, which allows one to balance enhanced state estimation against the loss in Coulombic capacity associated with adding MCMB. In summary, incorporating MCMB material in the graphite negative electrode provides an early warning before the battery reaches the end of discharge and facilitates voltage-based SOC estimation and retains good performance capability.

References

[1] M. Verbrugge, Adaptive characterization and modeling of electrochemical energy storage devices for hybrid electric vehicle applications , in: M. Schelsinger (Ed.), Modern Aspects of Electrochemistry No. 43: Modeling and Numerical Simulations I, first ed., Springer, 2009 (Chapter 8).
[2] M. Verbrugge, E. Tate, J. Power Sources 126 (2004) 236.
[3] B. Kang, G. Ceder, Nature 458 (2009) 190.
[4] N. Meethong, H.Y.S. Huang, W.C. Carter, Y.M. Chiang, A134, 2007.
[5] N. Meethong, H.Y.S. Huang, S.A. Speakman, W.C. Carter, Y.M. Chiang, Adv. Funct. Mater. 17 (2007) 1115.
[6] S.Y. Chung, J.T. Bloking, Y.M. Chiang, Nat. Mater. 1 (2002) 123.
[7] A. Yamada, H. Koizumi, S.I. Nishimura, N. Sonoyama, R. Kanno, M. Yonemura, T. Nakamura, Y. Kobayashi, Nat. Mater. 5 (2006) 357.
[8] C.S. Wang, U.S. Kasavajjula, P.E. Arce, J. Phys. Chem. C 111 (2007) 16656.
[9] C. Delmas, M. Maccario, L. Croguennec, F. Le Cras, F. Weill, Nat. Mater. 7 (2008) 665.
[10] A. Ait-Salah, J. Dodd, A. Mauger, R. Yazami, F. Gendron, C.M. Julien, Z. Anorg, Allg. Chem. 632 (2006) 1598.
[11] V. Srinivasan, J. Newman, J. Electrochem. Soc. 151 (2004) A1517.
[12] A.K. Padhi, K.S. Nanjundaswamy, J.B. Goodenough, J. Electrochem. Soc. 144 (1997) 1188.
[13] J. Wang, M.W. Verbrugge, P. Liu, J. Electrochem. Soc. 157 (2009) A185.
[14] Y. Kida, K. Yanagida, A. Funahashi, T. Nohma, I. Yonezu, J. Power Sources 94 (2001) 74.
[15] Y. Nishi, Mol. Cryst. Liq. Cryst. 340 (2000) 419.
[16] K. Yanagida, A. Yanai, Y. Kida, A. Funahashi, T. Nohma, I. Yonezu, J. Electrochem. Soc. 149 (2002) A804.
[17] M. Yoshio, R.J. Brodd, A. Kozawa, Lithium-ion Batteries , Springer, 2009.